Atherosclerotic Plaque Motion Analysis from Ultrasound Videos

S.E. Murillo*, M.S. Pattichis*, C.P. Loizou†, C.S. Pattichis‡,
E. Kyriacou§, A.G. Constantinides¶ and A. Nicolaides‖

*Department of Electrical and Computer Engineering
University of New Mexico, Albuquerque, NM-87131
email: smurillo, pattichis@ece.unm.edu
†Department of Computer Science
Intercollege Limassol Campus, CY-3507 Limassol, Cyprus
e-mail: christosl@lim.Intercollege.ac.cy
‡Department of Computer Science
University of Cyprus, CY1678 Nicosia, Cyprus
email: pattichi@ucy.ac.cy

§Cyprus Institute of Neurology and Genetics, CY1683, Nicosia, Cyprus
e-mail: ekyriac@ucy.ac.cy
¶Department of Electrical and Electronic Engineering, Imperial College
email: a.constantinides@imperial.ac.uk
‖Imperial College, London, England
University of Cyprus and Vascular Screening and Diagnostic Centre
Nicosia, Cyprus
e-mail: anicolai@cytanet.com.cy

***Abstract*— In this paper, we describe a collection of algorithms that are used to provide motion trajectory estimates from atherosclerotic plaque ultrasound videos. Our approach is based on the use of four different optical flow methods to estimate motion vectors (Horn and Schunk, Lucas, Nagel and Uras). To estimate the optimal motion estimation parameters, we perform hundreds of experiments on a Linux cluster, and further validate the results using synthetic simulations. Following motion estimation, we compute pixel motion trajectories over the plaque regions and vessel walls. Pixel trajectories are then used to assess plaque deformation.**

I. Introduction

Atherosclerosis is a disease of the large and medium size arteries, and it is characterized by plaque formation due to progressive intimal accumulation of lipid, protein, and cholesterol esters in the blood vessel wall [1], which reduces blood flow significantly. We expect that plaque and wall motion analysis will provide additional information regarding plaque instability.

We briefly summarize some related work. In [2], the authors computed optical flow estimates from 45 patients and reported a significant increase in the maximal discrepant surface velocity for the symptomatic cases, as compared to the asymptomatic cases. In [3], the authors used 3D intravascular ultrasound to provide a computational analysis of stress distribution.

Our study was motivated from a desire to extend traditional motion estimation methods into the development of reliable methods for trajectory estimation. To accomplish this, we are interested in developing realistic plaque motion models that are motivated from clinical experience. Using realistic motion models, we want to investigate the limits of traditional motion estimation methods. This paper describes an extension of our prior work reported in [4]. In [4], we described an earlier version of our system that relied on optical flow estimates from Horn and Schunk's method. In this paper, we consider four different optical flow methods and develop parameter optimization methods for each one.

We describe our method in Section II. Results are given in Section III and concluding remarks are provided in IV.

II. Methods

Our basic approach is to estimate motion vectors using optical flow and integrate the velocity estimates into video trajectories. This is summarized in three steps:

```
Step 1. Optimal Motion Estimation
Step 2. Use Runge-Kutta to integrate
Step 3. Display valid trajectories.
```

For motion estimation we considered a variety of optical flow methods [5]–[8]. We note that these optical flow methods have a number of parameters that can greatly affect the quality

of the motion estimates. We are interested in computing optimal estimates. For the optimization, we use synthetic video simulations.

Using the motion estimation velocities, we use a Runge-Kutta (4; 5) formula method [9] to provide motion trajectories throughout the video. We note that it is not always possible to compute valid motion trajectories throughout the video. Due to speckle noise, many motion velocity estimates maybe found to be invalid. Here, we note that all motion estimation methods allow us to assess the validity of the motion estimates. In summary, for the clinical videos, we establish the validity of the estimated trajectories based on: (i) the density of the estimated velocities, (ii) we require that trajectories remain valid throughout the video, (iii) estimation consistency and (iv) agreement with clinical expectations.

A. Optical Flow Methods

In [5], Horn and Schunk suggested a method for estimating video motion based on the assumption that image intensity remains constant

$$I\left(x,y,t\right)=I\left(x+\delta x,y+\delta y,t+\delta t\right). \tag{1}$$

Following a Taylor series expansion, assuming continuity in image intensity, they obtained the ill-posed, optical flow equation

$$I_x u+I_y v+I_t=0, \tag{2}$$

where $u\left(x,y\right),v\left(x,y\right)$ denote velocity estimates at pixel (x,y). Since (2) is ill-posed, Horn and Schunk imposed a derivative continuity constraint to solve (2) using

$$\iint\left(\alpha^2E_c^2+E_b^2\right)dx\ dy \tag{3}$$

where:

$$\begin{aligned}E_b^2&=I_xu+I_yv+I_t\\E_c^2&=\left(\frac{\partial u}{\partial x}\right)^2+\left(\frac{\delta u}{\partial y}\right)^2+\left(\frac{\partial v}{\partial x}\right)^2+\left(\frac{\partial v}{\partial y}\right)^2.\end{aligned} \tag{4}$$

To provide optimal motion estimates in (3), we search for an optimal value for the smoothness constraint parameter (α) and the σ-parameter of the spatiotemporal Gaussian pre-filter (see [5]).

Lucas and Kanade [6] suggested solving (2) using a weight function

$$\sum_{x\in\Omega}\left[W^2\left(x\right)\left(I_xu+I_yv+I_t\right)^2\right]. \tag{5}$$

For Lucas and Kanade, we search for the σ-parameter of the Gaussian smoothing filter and a threshold on the eigenvalues of the matrix A^TW^2A, where A contains the image gradients $A=[\nabla I(x_1),\ldots,\nabla I(x_n)]^T$, in order to identify unreliable estimates (see [6]).

In [7], Nagel introduced an oriented smoothness constraint to solve (2). He formulated the problem as one of minimizing

$$\begin{aligned}\iint E_b^2+\frac{\alpha^2}{\|\nabla I\|+2\delta}[(u_xI_y-u_yI_x)^2+\\(v_xI_y-v_yI_x)^2+\delta\left(u_x^2+u_y^2+v_x^2+v_y^2\right)]\,dxdy.\end{aligned} \tag{6}$$

For Nagel's method, we optimized for the value of α and the value of the σ parameter for the temporal pre-smoothing Gausian filter (see [7]).

Uras reformulated the motion estimation problem in terms of the Hessian of I. Locally, in 8×8 regions, he solves

$$\begin{bmatrix}I_{xx}&I_{yx}\\I_{xy}&I_{yy}\end{bmatrix}\begin{bmatrix}u\\v\end{bmatrix}+\begin{bmatrix}I_{tx}\\I_{ty}\end{bmatrix}=\begin{bmatrix}0\\0\end{bmatrix}. \tag{7}$$

Uras provides for a special method for dealing with the case when the Hessian is singular. For Uras' method, we searched for the optimal values for the σ parameters of the spatial and temporal Gaussian filters (see [8]).

B. Motion Trajectory Estimation Implementation

An MPI version of the optical-flow methods for motion estimation were implemented on the Los Lobos cluster (512 Pentium III processors) of the Albuquerque High Performance Computing Center. Estimates for each video frame were computed for many different values of the parameters.

III. Results

A. Synthetic Video Simulation Results

We considered synthetic simulations using three different videos. For the simulations, we begin with the first video frame of a clinical video and trajectory coordinate transformation equations for each pixel in the video. Then, to generate the rest of the video frames, we assume that the trajectory coordinate equations displace the original image intensities to the new coordinates, and use inverse interpolation to the image lattice to obtain the new frames. For the inverse interpolation we use cubic splines.

For the trajectories we use the following equations:

$$\begin{aligned}x(t)=A_h\sin(\frac{2\pi}{N}f_ht)+\frac{A_h}{2}\sin(\frac{2\pi}{N}(2f_h))\\+\frac{A_h}{3}\sin(\frac{2\pi}{N}(3f_h))\end{aligned} \tag{8}$$

$$\begin{aligned}y(t)=A_v\sin(\frac{2\pi}{N}f_vt)+\frac{A_v}{2}\sin(\frac{2\pi}{N}(2f_v)t)\\+\frac{A_v}{3}\sin(\frac{2\pi}{N}(3f_v)t)\end{aligned} \tag{9}$$

Here, we note that the amplitudes are decaying at a rate that is inversely proportional to the harmonic frequency. This is consistent with a discontinuity in the motion and has also been observed in the power spectra of the estimated trajectories (see [4] for details).

The simulation parameters are given in Table I. In Table I, horizontal frequency refers to f_h in (8), vertical frequency refers to f_v in (9). Similarly, horizontal amplitude refers to A_h in (8) while vertical amplitude refers to A_v in (9). For the lengths of the videos, we used $N=205,\ 180,\ 180$ for videos numbered 4, 5 and 17 respectively.

TABLE I

FREQUENCIES AND AMPLITUDES FOR THE FUNDAMENTAL COMPONENT.

Video Number	4	5	17
Horizontal Frequency (cycles per video-length)	8	7	4
Vertical Frequency (cycles per video-length)	8	7	10
Horizontal Motion Amplitude (pixels)	0.5	2.0	4.0
Vertical Motion Amplitude (pixels)	8.5	6.0	4.0

TABLE II

HORN'S METHOD MSE FOR SIMULATED VIDEO EXAMPLE

Horn MSE

	Sigma					
	0.75		**1.0**		**1.25**	
Alpha	U MSE	V MSE	U MSE	V MSE	U MSE	V MSE
0.50	0.146	0.355	0.172	0.381	0.201	0.493
0.75	0.121	0.341	0.144	0.370	0.170	0.479
1.00	0.105	0.334	0.126	0.366	0.149	0.471
1.25	0.094	0.332	0.113	0.365	0.135	0.468
1.50	0.086	0.333	0.104	0.366	0.124	0.466
1.75	**0.080**	**0.336**	0.097	0.368	0.116	0.466
2.00	0.076	0.339	0.092	0.371	0.109	0.467
2.25	0.072	0.344	0.087	0.374	0.104	0.469
2.50	0.070	0.348	0.084	0.378	0.100	0.471

1) Example of Optimization for Horn's Method: We present a parameter optimization example in Table II. This simulation refers to video #17, where the simulated motion is specified in Table I. The search region for the smoothness constraint in equation (3) was concentrated around $\alpha = 0.5 - 2.5$ and the values for the spatiotemporal filter ranged for $\sigma = 0.75 - 1.75$. Table II shows the MSE from which the optimal parameters were chosen returning a density of estimates of 90%.

B. Results on Synthetic Data

We present trajectory estimation results in Fig. 1. In Fig. 1(b) we present trajectory estimation results for three points, together with the actual motion (displayed in a solid line). In Fig. 1(b) we can see the relative accuracy of the approach. In any case, it appears that the phase changes in the actual trajectory are also reflected in the estimates. It is interesting to note that accurate estimates are obtained in frames 33 to 40, where the simulated motion is approximately linear. Significant errors appear at maximum displacement points. At these points, it appears that the trajectory estimates turn to either overshoot or undershoot the peaks.

C. Results on Clinical Videos

We computed motion trajectories on three clinical videos using the four motion estimation methods outlined in subsection II-A. We note that we did observe consistency in the trajectory estimates coming from the four different methods. In addition, only a small number of trajectories were labeled as being valid, in that they relied on valid motion estimates throughout the video. Three representative examples are shown in Figs. 2-4.

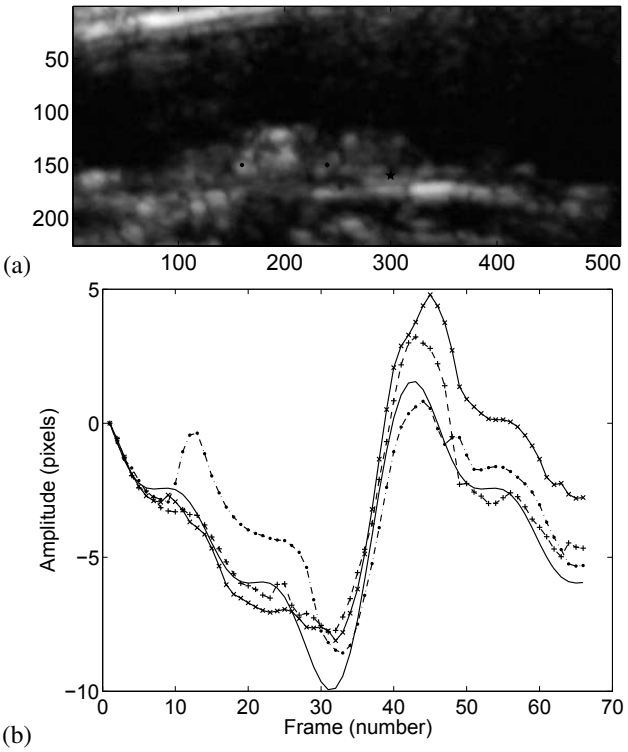

Fig. 1. Synthetic video motion estimation example for video #17 using Horn and Schunk's method. Using the optimal parameters shown in Table I, we computed trajectory estimates over three points. Here, we assumed that all three points undergo the same displacements. (a) First frame of the simulated video with plaque and artery wall. The three selected points consist of one point on the left-middle portion of the plaque ('x'), one near the middle of the plaque ('+'), and one close to the plaque-wall boundary (star). (b) Horizontal pixel motion for ground truth (solid line), point on the left-middle portion of the plaque (row=150, column= 160, 'x' line), point on the middle of the plaque (row=150, column= 1240, '+' line), and point close to the plaque-wall boundary (row=160, column= 300, 'o' line). Results over 66 frames.

For vide #4 we present trajectory estimation results in Figs. 2-3. In Fig. 2(b), we can see that the horizontal motion appears to be oscillatory. This motion appears to be in sync with cardiac motion. On the other hand, for the vertical motion in Fig. 2(c), we can see significant rise for the second point, lying on the plaque-wall boundary. The third point, lying below the plaque-wall boundary appears to oscillate, while the first point, lying on the plaque, also appears to be rising vertically. In Fig. 3(b) we can see that the horizontal motions for the two arterial points appear to be in sync with each other. Furthermore, for these arerial points, both the vertical and horizontal motions in Figs. 3(b)-(c) appear to be oscillatory. Here, we note that oscillatory motion is a sign of stability. On the other hand, the significant vertical motion in the plaque points suggests that that they exhibit a different response.

For video #17, we present trajectory estimation results in Fig. 4. From the vertical displacement results from Fig. 4(c), it appears that the plaque front is rising while the back of the plaque appears to be moving lower down. Overall, in terms of both the horizontal and vertical motion results, it appears that the front of the plaque appears to exhibit the

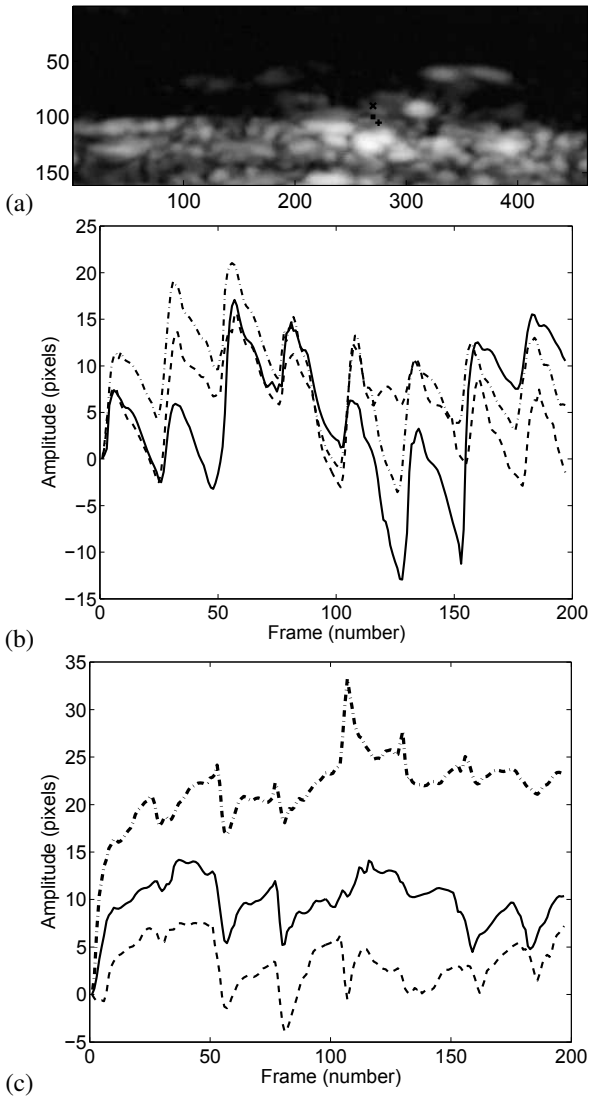

Fig. 2. Clinical video trajectory example for video #4. Motion estimation was based on the original method by Horn and Schunk. (a) Trajectories were estimated for three points shown on the first frame of the video (from top to bottom): Point-1 (90, 279) 'x', Point-2 (100, 270) 'square', and Point-3 (105,275) '+'. (b) Horizontal displacement motion plots: solid-line for Point-1, '-.-' line for Point-2 and '- -' line for Point-3. (c) Vertical displacement motion plots (same line styles as for (b)). Notice significant vertical displacements for points over the plaque and points close the plaque-wall boundary.

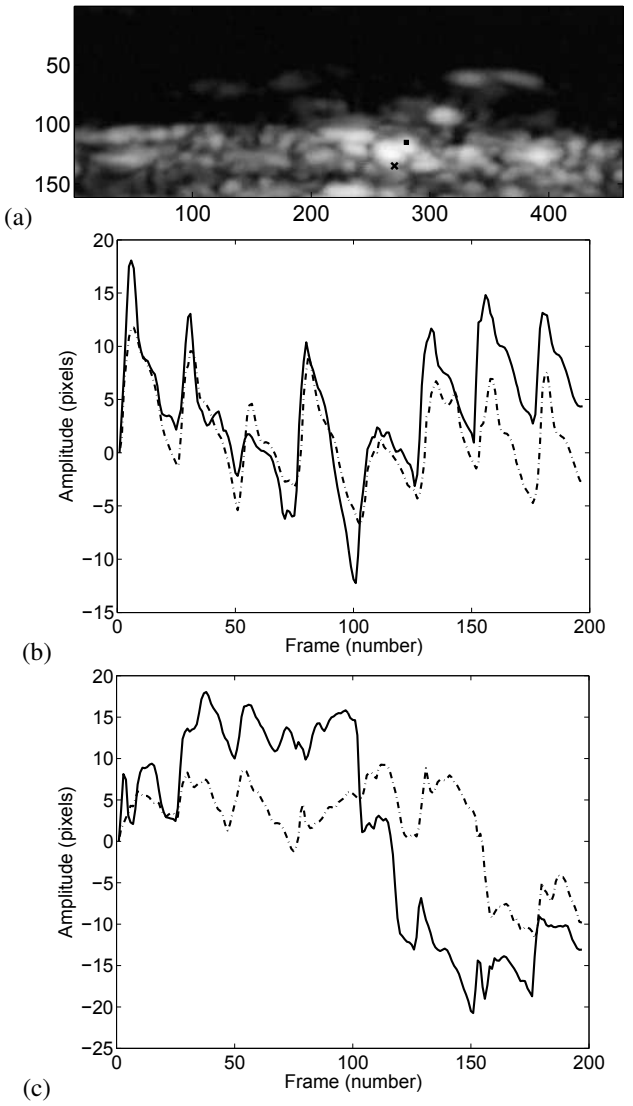

Fig. 3. Second clinical video trajectory example for video #4. Motion estimation was based on Uras's method. (a) Trajectories were estimated for two points shown on the first frame of the video (from top to bottom): Point-1 (135, 270) 'x', Point-2 (115, 280) 'square'. (b) Horizontal displacement motion plots: solid line for Point-1 and '-.-' line for Point-2. (c) vertical displacement motion plots (same line styles as for (b)). Notice that the horizontal motion trajectories appear to be in phase.

largest displacements.

IV. Concluding Remarks and Future Work

We believe that significant research is still needed to enable accurate motion trajectory estimation. A number of factors, such as image quality and speckle noise contribute to unreliable motion estimates. Despite all this, we do have confidence in the estimated, valid trajectories. We also observe that plaque regions exhibit significant displacements while wall and arterial regions exhibit stable, oscillatory motion.

Future work will be focused on developing a large database of symptomatic and asymptomatic videos, the implementation of a block-matching method for motion estimation [10], a phased-based approach [11] and the development of a new AM-FM based method for motion estimation. We are also investigating the use of total-variation methods for image de-noising, as well as the use of well-established methods for image de-speckling [12]. We want to apply these de-noising methods prior to motion trajectory estimation. It is expected that this approach will produce more accurate motion estimates. Furthermore, for computing the motion trajectories, we are investigating the use of particle filters.

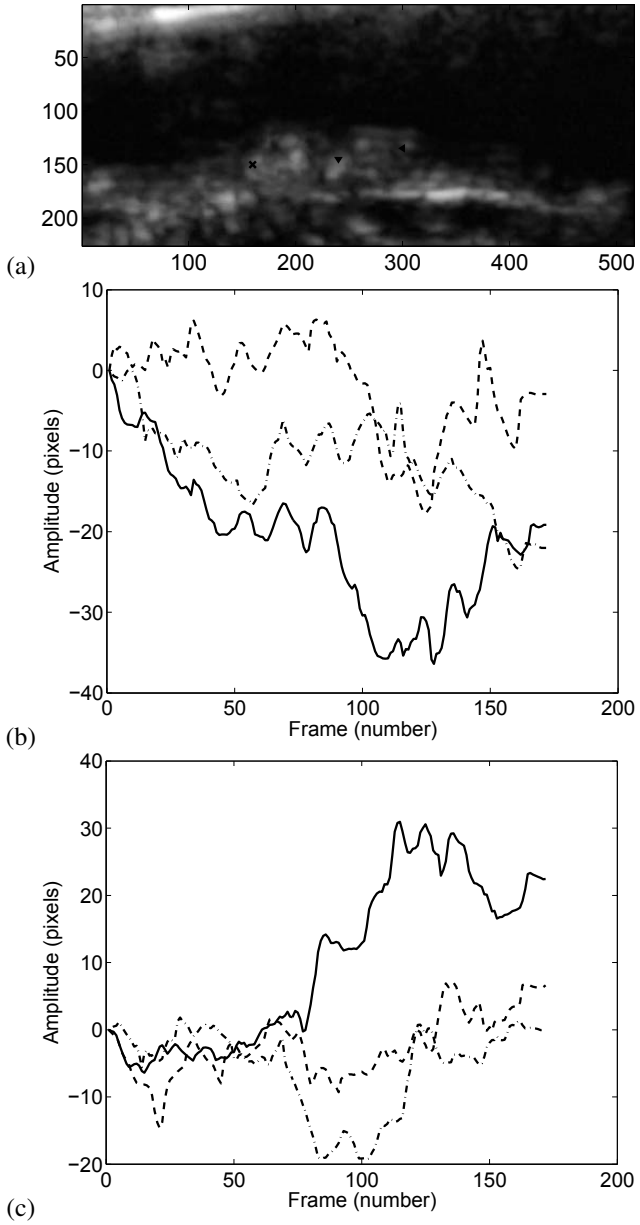

Fig. 4. Third clinical video trajectory example for video #17. Motion estimation was based on the original method by Horn and Schunk. (a) Trajectories were estimated for three points shown on the first frame of the video (from left to right): Point-1 (150, 160) 'x', Point-2 (145, 240) 'v' and Point-3 (135, 300) '¡'. (b) Horizontal displacement motion plots: solid line for Point-1, '- -' line for Point-2 and '-.-' line for Point-3. (c) vertical displacement motion plots (same line styles as for (b)).

ACKNOWLEDGMENT

This study was funded through the research promotion foundation of Cyprus, PENEK 2006, through the 6th annual program for the financing of research projects 2006, hosting an expatriate researcher, VISEMA, "Video Segmentation and Motion Analysis of the Atherosclerotic Carotid Plaque in Ultrasound Imaging", February 2006-February 2007, and the program for the financial support of new researchers, through the project entitled: "Intraoperative Computer Assisted Tissue Image Analysis" (CATIA), February 2006-February 2008.

REFERENCES

[1] C. Zarins, C. Xu, and S. Glagov, "Atherosclerotic enlargement of the human abdominal aorta," vol. 155, 2001, pp. 157–164.

[2] S. Meairs and M. Hennerici, "Four-dimensional ultrasonographic characterization of plaque surface motion in patients with symptomatic and asymptomatic carotid artery stenosis," *Stroke*, vol. 30, no. 9, pp. 1807–1813, Sep. 1999.

[3] K. Imoto, T. Hiro, T. Fujii, A. Murashige, Y. Fukumoto, G. Hashimoto, T. Okamura, J. Yamada, K. Mori, and M. Matsuzaki, "Longitudinal structural determinants of atherosclerotic plaque vulnerability a computational analysis of stress distribution using vessel models and three-dimensional intravascular ultrasound imaging," *J. Am. Coll. Cardiol.*, vol. 46, pp. 1507–1515, Sept. 2005.

[4] S. Murillo, M. Pattichis, C. Loizou, C. Pattichis, and E. Kyriakou, "Atherosclerotic plaque motion trajectory analysis from ultrasound videos," in *IEEE Int. Special Topic Conf. on Inform. Technology in Biomedicine*, Ioannina, Greece, Oct. 2006, pp. 1–5.

[5] B. Horn and B. Schunck, "Determining optical flow," *Artificial Intelligence*, vol. 17, pp. 185–203, 1981.

[6] B. Lucas and T. Kanade, "An iterative image registration technique with an aplication to stereo vision," in *Proc. DARPA IU Workshop*, 1981, pp. 121–130.

[7] H. Nagel, "Displacement vectors derived from second-order intensity variations in image sequences," *Computer Vision Graphics and Image Processing*, vol. 21, pp. 85–117, 1983.

[8] S. Uras, "A computational approach to motion perception," *Biol. Cybern*, vol. 60, pp. 79–97.

[9] J. Dormand and P. Prince, "A family of embedded runge-kutta formulae," *J. Compu. App. Math*, vol. 6, pp. 19–26, 1980.

[10] P. Anandan, "A conputational framework and an algorithm for the measurement of visual motion," *International Journal of Computer Vision*, vol. 2, pp. 283–310, 1989.

[11] D. J. Fleet and A. D. Jepson, "Computation of component image velocity from local phase information," *International Journal of Computer Vision*, vol. 5, no. 1, pp. 77–104, 1990.

[12] C. Loizou, C. Pattichis, C. Christodoulou, R. Istepanian, M. Pantziaris, T. Tyllis, and A. Nicolaides, "Comparative evaluation of despeckle filtering in ultrasound imaging of the carotid artery," *IEEE Trans. Ultrasonics Ferroelectrics and Frequency Control*, vol. 52, no. 10, pp. 1653–1669, 2005.